Version: Accepted Version

Article:

Liu, C, Chen, X, Banwart, SA et al. (2021) A novel permeable reactive biobarrier for ortho-nitrochlorobenzene pollution control in groundwater: experimental evaluation and kinetic modelling. Journal of Hazardous Materials, 420. 126563. ISSN: 0304-3894

https://doi.org/10.1016/j.jhazmat.2021.126563

A novel permeable reactive biobarrier for *ortho*-nitrochlorobenzene pollution control in groundwater: experimental evaluation and kinetic modelling

Cuicui Liu[a,b], Xiaohui Chen[b], Steven A. Banwart[c,d], Wenchao Du[e], Ying Yin[a], Hongyan Guo[a,f]*

[a]State Key Laboratory of Pollution Control and Resource Reuse, School of the Environment, Nanjing University, Nanjing, 210023, China
[b]School of Civil Engineering, University of Leeds, Leeds, LS2 9JT, UK
[c]School of Earth and Environment, University of Leeds, Leeds, LS2 9JT, UK
[d]Global Food and Environment Institute, University of Leeds, Leeds, LS2 9JT, UK
[e]School of the Environment, Nanjing Normal University, Nanjing, 210023, China
[f]Joint International Research Centre for Critical Zone Science-University of Leeds and Nanjing University, Nanjing University, Nanjing, 210023, China
*Correspondence: Hongyan Guo, tel.: +8613813945566, fax: +86-25-89680263
E-mail: hyguo@nju.edu.cn

Abstract

Three novel permeable reactive barrier (PRB) materials composed of Cu/Fe with 0.24% and 0.43% (w/w) Cu loadings or Fe^0 supported on wheat straw were prepared (termed materials E, F and G). These materials exhibited excellent pollutant removal efficiency and physical stability as well as the ongoing release of organic carbon and iron. Column experiments showed that materials E, F and G removed almost 100% of *ortho*-nitrochlorobenzene (*o*-NCB) from water. The rates of iron release from the E and F columns exceeded those from column G but this had no significant effect on *o*-NCB removal. The bacteria that degraded *o*-NCB in E and F were also different from those in G. The levels of these bacteria in the columns were higher than those in the initial materials, with the highest level in column E. The simultaneous reduction and microbial degradation of *o*-NCB was observed, with the latter being dominant. A kinetic model was established to simulate the dynamic interactions and accurately predicted the experimental results. Organic carbon from the wheat straw supported the majority of the biomass in each column, which was essential for the bioremediation process. The findings of this study suggest an economically viable approach to mitigating *o*-NCB pollution.

Keywords: *o*-NCB; Reduction; Biodegradation; PHREEQC; Kinetics

1. Introduction

The compound *ortho*-nitrochlorobenzene (*o*-NCB) is a known human carcinogen, and is also associated with splenomegaly and cardiovascular diseases (Xu et al., 2014; Zhang et al., 2011). Even so, this chemical is widely used in industrial water systems to prevent the formation of slime. In 2006 the combined production of *o*-NCB and *p*-nitrochlorobenzene (*p*-NCB) in China was approximately 5.25×10^5 t, which accounted for 65% of the total worldwide production (Chen et al., 2006). The *o*-NCB has also been listed as a priority environmental pollutant by US Environmental Protection Agency and is subject to regulatory control in China.

As a result of the electron-withdrawing nature of the nitro group and chlorine atom on the aromatic ring, *o*-NCB is relatively recalcitrant in aquatic environments. There are some available oxidation or reduction processes, including hydrogen peroxide/persulfate oxidation (Liu et al., 2016), ozonation (Li et al., 2009) and synergistic catalytic reduction using bioPd and Shewanella oneidensis MR-1 (Kong et al., 2017), that have been used for the removal of *o*-NCB. However, these processes are expensive and can result in the release of secondary pollutants. In recent years, permeable reactive barriers (PRBs) have become a promising means of groundwater remediation (Ebert et al., 2006). Zero-valent iron (Fe^0) is a nontoxic, inexpensive and effective reductive PRB material, and has increasingly been utilized to remediate groundwater contaminated with chlorinated organic compounds (Henderson and Demond, 2007). Fe^0 can also be modified with another metal such as Pt, Ni or Cu, called bimetallic particles, that are efficient at degrading various organic pollutants (Hosseini et al., 2011). Among the possible second metals, Cu is relatively inexpensive and thus has a wide range of potential applications (Karami et al., 2018; Zhang et al., 2019b). In addition, Cu/Fe materials have been shown to exhibit high levels of reactivity even after prolonged storage (Ren et al., 2017), and to efficiently remove 2,4-dichlorophenol (Pan et al., 2019), 1,2,4-trichlorobenzene (Cao et al., 2011), 2,4-dinitroanisole (Kitcher et al., 2017) and nitroarenes (Karami et al., 2018) via reductive degradation.

Biological PRBs are another economical and effective approach to groundwater remediation (Gibert et al., 2019). The metabolic activities of these microbes and the structure of the associated microbial communities are known to be affected by organic carbon acting as sources of both carbon and energy (Chen et al., 2017). Yin et al. (2012) reported that the presence of certain organic substrates improved the removal rate of *p*-NCB with microbes by promoting a bio-reduction process. In a previous study, our group accessed the potential of wheat straw as an additional carbon source for the remediation of groundwater contaminated with phenanthrene (Liu et al., 2019). As a continuation of that prior work, the present research examined the role of wheat straw as a carbon and energy source to promote the biological reductive dechlorination of *o*-NCB. The degradation of this chemical can also be enhanced by combining reduction by Fe^0 with microbial degradation, and Yin et al. (2012) and Zhu et al. (2013) reported that co-reduction by Fe^0 and microorganisms significantly increased the extent of *p*-NCB removal. Lin et al. (2011), Xu et al. (2011) and Zhu et al. (2015) have also shown that the biodegradability of *o*-NCB is significantly enhanced in the presence of Fe^0.

Based on the above, the objective of the present study was to evaluate the application of new PRB materials based on both Fe^0 reduction and biodegradation to the *in situ* remediation of groundwater containing *o*-NCB. These trials employed long-term column experiments. Additionally, we developed a new model based on the PHREEQC computer program to study the combined mechanism involving reduction by Fe^0 and microbial degradation, to obtain a deeper understanding of the *o*-NCB removal mechanism in columns containing three different PRB materials.

2. Materials and methods

2.1. Experimental work

2.1.1. Preparation of PRB materials

Two different Cu loadings (0.24% and 0.43%, w/w) were applied to the surface of Fe^0 particles having a mean particle size of approximately 74 μm (> 99% purity, Nanjing Jukang Biotec Co., Ltd.). The resulting materials are referred to herein as Cu/Fe-1 and Cu/Fe-2. These were obtained by adding 2 g of Fe^0 particles to 10 and 18 mL, respectively, of an aqueous 1000 mg/L $CuCl_2$ solution, followed by vigorous stirring for 30 min to ensure that the Fe^0 surfaces were covered with Cu layers. During this process, the redox reaction between the Cu^{2+} and Fe^0 was:

$$Fe^0 + Cu^{2+} \rightarrow Fe^{2+} + Cu^0. \qquad (1)$$

The resulting Cu/Fe products were washed three times with deionized water and then dried at 25 °C.

Three novel PRB materials included the Cu/Fe-1, Cu/Fe-2 and Fe^0, termed materials E, F and G, respectively. These were produced in the form of pellets, each having a core, a packed layer and an outer shell, using a rolling granulation method with sodium alginate in water as a binder. The core of each sample was made of wood while the packed layer consisted of wheat straw, attapulgite, diatomite and either Cu/Fe-1, Cu/Fe-2 or Fe^0. This layer provided both carbon and iron. The porous outer shell was made from attapulgite, diatomite and Portland cement and was intended to increase the hardness of the PRB. The basic physical characteristics of the components of PRB materials are summarized in Table S1. The diameters of these pellets were measured with a caliper, and were found to range from 0.8 to 1.0 cm.

2.1.2. Column experiments

The experimental trials used three glass columns (length: 50 cm, inner diameter: 4 cm) equipped with sampling ports at the top and bottom as well as four vertical sampling ports (SP1-SP4) situated at 10 cm intervals along the column. Each column was homogenously packed with the mixture of one of the three PRB materials together with quartz sand (at a 1:1, v/v, ratio to the PRB materials). The mixture was bounded by 5 cm layers of quartz sand at the top and base of the column. Trials in which deionized water flowed through the columns were used to estimate the residence time and velocity in reactive media (Moustafa, 2019). The ultra-pure water was used to prepare 10 mg/L *o*-NCB solution. Nitrogen gas was pumped through the feed solution to maintain anaerobic conditions. The initial pH value of the feed solution was about 6.7 and the concentration of oxygen was less than 0.1 mg/L. In each experiment, the 10 mg/L *o*-NCB solution was pumped upward through the column at a constant flow rate of 126.9

μL min^{-1} to replicate the flow rate of 0.48 m d^{-1} expected to occur during the remediation of groundwater. Each trial was performed over a span of 460 d in a dark environment at room temperature (20±5 °C). Detailed information regarding the E, F and G columns is presented in Table S2.

2.1.3. Analytical methods

Samples of the effluents from each column were centrifuged at 10,000 rpm for 15 min, after which the supernatant was analyzed. The concentrations of *o*-NCB and its degradation product *o*-chloroaniline (*o*-CAN) were determined in each aliquot using high performance liquid chromatography (HPLC, model 1200, Agilent, USA), employing a Supelco Discover C-18 reverse phase column (25 cm × 4.6 mm particle size = 5 μm) together with a 75:25 methanol/water mobile phase at 1.0 mL min^{-1} and an ultraviolet detector set at 254 nm. The pH was measured using a portable analyzer (Orion 5 Star, Thermo, USA). The total organic carbon (TOC) concentration in each sample was determined using an Aurora 1030D meter (OI Analytical, US). The total iron values were obtained via atomic absorption spectroscopy (Thermo M 6, USA), while chloride ions resulting from the dechlorination of *o*-NCB were quantified using ion chromatography (Dionex ICS-1100, Thermo, USA). The detection limits for *o*-NCB, *o*-CAN and chloride ions using these analytical techniques were 0.01 mg/L, 0.05 mg/L and 0.1 μg/L, respectively.

The morphologies of the initial PRB materials and of PRB samples collected from the three columns after 460 d were characterized by environmental scanning electron microscope (ESEM, FEI Quanta 250 FEG, USA). The surface elemental distributions were ascertained using energy dispersive X-ray spectroscopy (EDS, Oxford Aztec X-Max^N 80, USA) with a silicon drift detector. Materials E, F and G before and after column experiments were analyzed by X-ray Photoelectron Spectroscopy (XPS, Thermo Scientific Escalab 250) with Al Kα X-ray excitation source under the pressure of ~2×10^{-9} Pa to figure out the formation of iron corrosion products. Surface charging were corrected with C 1s peak at 284.6 eV as the reference. XPS spectra were treated by a Shirley-type background subtraction and fitted with mixed Gaussian-Lorenzian functions using a standard program for data processing.

2.1.4. Analysis of microbial communities

Samples of materials E, F and G before use were also placed in sealed containers and stored at -80 °C to inhibit microbial growth. Additional samples were obtained from columns E, F and G from sampling ports SP1 to SP4 after the 460 d trial. DNA was extracted from 0.4 g subsamples using a MOBIO PowerSoil® DNA Isolation Kit and the V3-V4 regions of the bacterial 16S rRNA gene were amplified using 338F (5′-ACTCCTACGGGAGGCAGCA-3′) and 806R (5′-GGACTACHVGGGTWTCTAAT-3′) as primers. Each PCR amplification reaction mixture had a final volume of 60 μL and included 0.5 U of Ex Taq (TaKaRa, Dalian), 10 mM dNTP, 50 μM primer and 10 ng of genomic DNA extracted from the E, F and G samples. PCR amplification was performed in conjunction with thermal cycling. The cycle comprised an initial temperature of 94 °C for 5 min, followed by 30 cycles of 94 °C for 30 s, 52 °C for 30 s and 72 °C for 30 s, with a final hold at 72 °C for 10 min. The PCR products were determined by electrophoresis in a 1% agarose gel. The mixed PCR products were purified using an EZNA Gel Extraction Kit (Omega, USA). Sequencing libraries were generated using the NEBNext® Ultra™ DNA Library Prep Kit for Illumina® (New England Biolabs, USA) and index codes were added. Purified amplicons were sequenced on an Illumina Hiseq 2500 platform and 250 bp paired-end reads were generated. The raw reads were deposited in the NCBI Sequence Read Archive (SRA) database with accession numbers SRP194147.

2.2. Modelling approach

Fig. 1 presents a diagram summarizing the iron-based reduction, microbial degradation and consumption of dissolved organic carbon that occurred in the columns. The stoichiometries associated with the geochemical reactions simulated in the model and the model transport parameters are provided in Table 1 and Table S3, respectively. The reaction and kinetics parameters (Table 2) were obtained from either experimental trials or the literature, and these values were used to define the model. Considering the context of real-world applicability, the modelling was also extended to apply to *o*-NCB contaminated aerobic groundwater and the predicted results were analyzed in supporting information (Table S5, Table S6 and Figure S2).

2.2.1. Iron-based reduction of *o*-NCB

The degradation of the *o*-NCB by either the Fe^0 or Cu/Fe particles was found to correspond to a pseudo-first order reaction, when the concentration of the particles was excessive in the reaction. The reaction rates (mol L^{-1} s^{-1}) of the organic compounds during this remediation could be expressed as (Dong et al., 2011; Huang et al., 2016):

$$R_{o-NCB} = -k_1 C_{o-NCB} \qquad (2)$$

and

$$R_{o-CAN} = k_1 C_{o-NCB} - k_2 C_{o-CAN}, \qquad (3)$$

where C_{o-NCB} is the *o*-NCB concentration (mol L^{-1}), C_{o-CAN} is the *o*-CAN concentration (mol L^{-1}), and k_1 and k_2 are the corresponding reaction rate constants (s^{-1}). The values of k_1 and k_2 were determined based on the static experimental data (Table S4). The iron mass-normalized *o*-NCB removal of materials E, F and G were shown in Figure S4.

2.2.2. Microbial degradation for *o*-NCB

Microbial processes were determined to be the primary drivers of mass transfer and transformations that occurred during the present experiments. On this basis, double Monod kinetics were used to simulate the biodegradation of *o*-NCB (Malaguerra et al., 2011), according to the equation:

$$R_S = -\frac{\mu_{max} X}{Y_X} \frac{C_{H_2}}{C_{H_2} + K_{H_2}} \frac{S}{S + K_S \, (1+\frac{C_1}{K_1})}, \qquad (4)$$

where R_s is the rate of substrate consumption (mol L^{-1} s^{-1}), μ_{max} is the maximum growth rate (s^{-1}), X is the biomass concentration (mol L^{-1}), Y_X is the microbial yield coefficient (mol biomass C/mol substrate C), C_{H_2} is the concentration of dissolved molecular hydrogen acting as an electron donor (mol L^{-1}), K_{H_2} is the half-maximum rate hydrogen concentration (mol L^{-1}), S is the aqueous concentration of the substrate (o-NCB) acting as an electron acceptor (mol L^{-1}), K_S is the half-maximum rate substrate concentration (mol L^{-1}), C_1 is the concentration of o-CAN, the degradation product of o-NCB (mol L^{-1}), and K_1 is the relative inhibition constant (mol L^{-1}). The double Monod kinetics parameters were taken from prior studies related to the removal of chlorinated or organic compounds (Acharya et al., 2019; Akobi et al., 2017; la Cecilia and Maggi, 2016; Malaguerra et al., 2011; Schafer et al., 1998), so as to obtain the best fit of the model to the experimental results. The change in the substrate was related to the amount of biomass according to the relationship:

$$R_{Cells} = -Y_X R_S - bX, \qquad (5)$$

where R_{Cells} is the rate of cell growth (mol C L^{-1} s^{-1}) and b is the first-order microbial decay coefficient (s^{-1}). The value of b was obtained from a report by Chen and McTernan (1992), who suggested a b value for bacteria. The carbon content of the biomass was estimated on the basis of the carbon content of a bacterial cell (9.4×10^{-14} g C/cell) (Acharya et al., 2019).

2.2.3. The consumption of organic carbon

In this work, the microbes were able to use organic carbon as sources of both carbon and energy, and the organic carbon were defined in our modelling simulations as CH_2O. The total available organic carbon in columns E, F and G was determined to be 41.08, 40.25 and 40.75 g C, respectively. In addition, using the hydraulic conductivity and porosity of the columns (Table S2), we calculated that 51.71, 53.25 and 52.37 L of groundwater, respectively, flowed through columns E, F and G every year. The calculated average annual releases of total organic carbon from columns E, F and G were 2.08, 1.94 and 2.05 g C, respectively. Therefore, the time span for carbon release from each of these columns was about 20 y. The degradation of solid organic hydrocarbons under anaerobic conditions was summarized by the equation (Xu et al., 2007):

$$3CH_2O + H_2O \rightarrow CH_3COOH + CO_2 + 2H_2. \qquad (6)$$

In this simplified model, the production of CO_2 was correlated with the energy used by the bacteria that mediated the decomposition process. The dissolved organic carbon degradation kinetics were assumed to be Monod type (Dalaei et al., 2020; King et al., 2012; Lashermes et al., 2020), such that the related equation was:

$$R_s = -\frac{\mu_{max}X}{Y_X}\frac{C_{oc}}{C_{oc}+K_{oc}}, \qquad (7)$$

where R_s is the rate of substrate consumption (mol L^{-1} s^{-1}), C_{oc} is the concentration of dissolved organic carbon (mol L^{-1}), and K_{oc} is the half-maximum rate organic carbon concentration (mol L^{-1}). The parameters for Monod kinetics were obtained from prior reports concerning the consumption of organic compounds (Akobi et al., 2017; Carboneras et al., 2017; la Cecilia and Maggi, 2016; Vasiliadou et al., 2015; Verce et al., 2000). The support of microbial growth by dissolved organic carbon could be expressed by equation (5). In the present modelling, we assumed that the Cu/Fe in columns E and F was able to reductively transform *o*-NCB to produce chloride ions, while the Fe^0 in column G could only reduce *o*-NCB to *o*-CAN without the production of chloride ions (Figure S3) (Xu et al., 2020). We also assumed that columns E, F and

G could continuously provide a carbon source over a period of 20 years. In this model, hydrogen produced by the Cu/Fe and Fe^0 through reactions with water served as the electron donor for the biodegradation of *o*-NCB.

3. Results and discussion

3.1. *o*-NCB transformation in columns E, F and G

Column experiments were performed to simulate the PRB system and to evaluate the feasibility of remediating groundwater contaminated with *o*-NCB. Figs. 2a-e present the simulated and experimental results regarding the levels of *o*-NCB, *o*-CAN, chloride ions, total iron and TOC over time in the effluent from columns E, F and G.

The only difference of materials E, F and G was the reductants in the packed layer. The reductants of the three materials were Cu/Fe with 0.24% Cu loadings, Cu/Fe with 0.43% Cu loadings, and Fe^0, respectively. As can be seen from Fig. 2a, the concentration of *o*-NCB was lower in column F compared with columns E and G in the initial stage of the remediation process. This result can possibly be ascribed to the catalysis role of Cu and the enhancement of electron release on Fe surface by the potential difference between Cu and Fe (Cao et al., 2011; Fang et al., 2018; Shih et al., 2009), which accelerated the reduction of *o*-NCB. However, column F did not exhibit long-term advantage in the removal of *o*-NCB, suggesting that the faster release of iron was not more beneficial. Furthermore, iron reduction was only one of the mechanisms by which *o*-NCB was degraded in the columns, because this compound also underwent biodegradation as the levels of degrading bacteria increased. These data also demonstrate that close to 100% of the contaminant was removed in all three columns, and that the modelling results were in good agreement with the experimental data. The model predicted that the *o*-NCB concentration would initially be lower in columns E and F and that very low levels of this compound would remain in all three columns during prolonged operation. Fig. 2b indicates that *o*-CAN was only detected in very low concentrations at the initial stage, and so the decomposition efficiency for this pollutant was close to 100% in each case. The simulated *o*-CAN concentrations were also generally in good agreement with the actual observations. However, the *o*-CAN concentrations in column G were slightly higher than those in columns E and F, presumably because our model did not consider the dechlorination of *o*-CAN based on iron reduction in this column. Fig. 2c plots the changes of chloride ion concentrations in the effluents of all three columns. The *o*-NCB degradation rates could be determined based on these data (Wu et al., 2009). The chloride ion concentrations in the effluents from the columns were between 0.036 and 0.048 mmol/L throughout the entire experimental time span. The experimental *o*-CAN concentrations in the samples from columns E, F and G were also all very low, indicating that this compound was almost completely dechlorinated in each column. The chloride ion concentration in the effluent of each column was predicted to be approximately 0.06 mmol/L, although the experimental values were lower. This discrepancy can possibly be ascribed to the formation of a complex between iron and chloride ions (Böhm et al., 2015), the capture of chloride ions by the wheat straw (Qiu et al., 2020) or the formation of other intermediate products that reduced the chloride ion levels leaving the columns. Yin et al. (2012) reported a maximum *p*-NCB removal of 95.6% using Fe^0 and a mixed anaerobic culture, and this value was exceeded by the new PRB system reported herein based on the degradation of *o*-NCB. These results suggest that materials E, F and G were all able to effectively remove *o*-NCB from groundwater, and that the associated degradation product (*o*-CAN) was also almost completely degraded in each case. Material G with Fe^0 for *o*-NCB removal was satisfactory in the present confined experimental study. However, when the PRB materials are used for *in situ* remediation of *o*-NCB contaminated aerobic groundwater, materials E and F with Cu/Fe may have an advantage over material G with Fe^0 due to the faster consumption of oxygen (Figure S2). In addition, when the hydrochemical conditions of groundwater are unfavorable for microbial growth during the early stages, the Cu/Fe reductively dechlorination is very important for removing *o*-NCB. Pan et al. (2019) reported that Cu was a cost-effective material to be used for modifying Fe^0 to prepare the Cu/Fe bimetal and also Cao et al. (2011) reported that the bimetallic Cu/Fe was preferred choice especially for *in situ* remediation when balancing economical factor with reduction efficiency. Further studies are currently under way to fully understand the practical applications of the PRB materials in different groundwater environments.

3.2. Total iron and TOC variations

The variations in the total iron concentrations over time are plotted in Fig. 2d, from which it is evident that the release of iron was relatively slow in all three columns prior to the 100 d point. The iron concentration in the effluent from column G ranged from

0.002 to 0.05 mmol/L, while the levels in samples from columns E and F ranged from 0.003 and 0.005 mmol/L to 0.13 and 0.25 mmol/L, respectively. These data confirm that the rates of release of iron from the latter two columns exceeded that from column G, possibly because the potential difference between Cu and Fe enhanced electron transfer on Fe surface, which accelerated the release of iron. The predicted total iron concentrations generally agreed very well with the observed values up to day 460. Although the concentrations of iron in columns E and F were higher than that in column G, the former two units did not remove *o*-NCB more rapidly, suggesting that the iron concentration did not significantly affect the decomposition of the contaminant in this PRB system. Prior studies have suggested that Fe^0 promotes the reduction of nitro compounds but does not dechlorinate chlorine aromatics (Agrawal and Tratnyek, 1995; Zhu et al., 2013). Huang et al. (2016) assessed the removal of nitrobenzene and chlorobenzene by Fe^0 and also reported a lack of dechlorination reactions. Even so, the transformation of *o*-NCB into *o*-CAN using Fe^0 could significantly mitigate the toxicity of the former compound and promote further degradation in subsequent biological processes (Xu et al., 2011). Additionally, it should be noted that a column containing Fe^0 has the potential to exhibit decreased long-term performance resulting from the formation of a precipitate (Farrell et al., 2000; Henderson and Demond, 2007). Even so, in the present work, a high level of *o*-NCB removal was obtained from all columns throughout the experiment.

Fig. 2e presents the variations in the TOC concentrations in the effluents of columns E, F and G over time. The influent TOC concentration was determined to be approximately 26.87 mmol/L, while the levels in samples from the columns increased from 18.7, 16.5 and 18.4 mmol/L to 29.9, 34.5 and 31.1 mmol/L over the first 60 d, respectively. These values subsequently decreased to 15.5, 20.2 and 15.1 mmol/L on day 215, respectively, but otherwise remained relatively stable with values between 5.4 and 22.9 mmol/L. These results are attributed to the release of organic carbon from the PRB materials, primarily as the soluble fraction of the wheat straw was released during the early stages. The TOC levels after that point were largely dependent on the mineralization of the insoluble pool of straw (Cogle et al., 1989). In the modelling process, we assumed that organic carbon could be released continuously over 20 years and would support microbial growth throughout this time span. Thus, the predicted TOC concentrations conformed to the same trend as the experimental values. That is, the TOC level first increased, then gradually decreased as the available carbon was consumed. The organic carbon present during remediation can affect the structure of the microbial communities and also provide a carbon source for the growth of microbes (Chen et al., 2017). Moreover, organic carbon can serve as an electron donor for the biodegradation of *o*-NCB (Chang et al., 2018; Nguyen et al., 2016). Park et al. (1999) and Kuhlmann and Hegemann (1997) reported that the presence of organic substrates increased the *p*-CNB removal rate, which was attributed to the utilization of the organic materials by the microorganisms. Therefore, the presence of organic carbon in the present study may have helped to maintain the population of bacteria responsible for pollutant decomposition as the *o*-NCB concentration varied over time.

The variations of pH caused by Fe^0 corrosion and anaerobic digestion of wheat straw were shown in Figure S1. The initial pH value of the feed solution was about 6.7. The pH increased in the effluent from the three columns during the early stages, which were between 8.2 and 8.4. This result can be attributed to Fe^0 reduction reaction producing hydroxide ions. The attapulgite and Portland cement may also have contributed to the increase in the pH. After 61 days, the pH decreased and changed in the range of 6.5 and 7.6. This is because that the digestion of the insoluble pool of wheat straw in anaerobic environment could produce organic acids such as acetic acid and propionic acid (Gao et al., 2020). The generation of OH^- ions and organic acids caused groundwater pH changes, which played a buffering role for the later stable and more neutral environment. The PRB system may have the capacity of buffering acidic or alkaline groundwater to reduce the impact of different pH values. The different ionic strength in groundwater may also affect the application of Fe^0 (Esfahani et al., 2014; Li et al., 2017). We will further research the influence of different pH and ionic strength on practical application of the PRB materials in the future studies.

3.3. ESEM-EDS and XPS analysis

ESEM images were acquired to assess changes in the surface morphology of materials E, F and G before and after the experiment (Figs. 3E0-G0, E1-G1). Initially, each sample had a smooth surface (Figs. 3E0-G0) but, after 460 days, the surfaces showed mushroom-like structures (Figs. 3E1-G1) and obvious microstructural changes. EDS was used for elemental analyses to establish the spatial distributions of the main elements in these materials, and Figs. 3a-p present the results. The carbon maps in Figs.

3a-f show relatively homogeneous distributions of this element, as do the iron maps in Figs. 3g-l. Figs. 3m-p also confirm relatively homogeneous copper distributions. These data indicate that carbon, iron and copper were present in materials E, F and G. Compared with the initial materials (Figs. 3a, c, e, g, i, k, m and o), the intensities of all three elements in all three materials were reduced after the experiment (Figs. 3b, d, f, h, j, l, n and p), indicating that C, Fe and Cu had been released. Additionally, the detailed XPS spectra for the region of Fe 2p was shown in Fig. 4. Fe(0) at 706.6 eV was only observed in initial PRB materials and disappeared after column experiments, which suggested that Fe(0) was converted to other valence states during the experimental process. Peaks at 710.4 eV and 713.8 eV corresponded to Fe $2p_{3/2}$ of Fe(II) and Fe(III), respectively, and peaks at 723.8 eV were assigned to Fe $2p_{1/2}$ of Fe(III) (Zhang et al., 2019a; Zhang et al., 2019b).

3.4. Changes in microbial community structures

The microbial community structures in the initial PRB materials and solid samples from columns E, F and G were shown in Fig. 5a. The bacterial phyla were dominated by *Firmicutes* (27.9%−85.4%), *Proteobacteria* (2.9%−44.2%), *Actinobacteria* (0.2%−32.4%), *Verrucomicrobia* (0.03%−11.5%), *Acidobacteria* (0.15%−4.3%), *Bacteroidetes* (0.25%−2%) and *Chloroflexi* (0.12%−3%). Studies have reported that *Firmicutes* and *Bacteroidetes* played an important role in hydrolysis and acidogenesis during anaerobic digestion of straw (Ziganshin et al., 2013), which caused the formation of organic acids. Furthermore, large changes in community composition occurred with (columns E and F) or without (column G) Cu. Columns E and F showed a higher abundance in phylum *Proteobacteria* than that in column G. Conversely, the phyla *Firmicutes*, *Actinobacteria*, *Verrucomicrobia*, *Acidobacteria* and *Chloroflexi* in columns E and F had a lower abundance than that in column G. Ahmed et al. (2020) found that the abundance of phylum *Proteobacteria* presented an increase within Cu-treated communities, while, the abundance had a decrease in the phyla *Actinobacteria* and *Chloroflexi*. Other previous studies also reported that *Proteobacteria* was the dominant phylum under the condition of Cu exposure (Fagnano et al., 2020; Ouyang et al., 2016). Based on unweighted UniFrac metrics, principle coordinated analysis (PCoA) was performed to compare the bacterial communities among different samples (Fig. 5b). The first and second axes explained 21.78% and 17.03% of the community variance, respectively. The samples of SP1-4 ports from column G formed a distinct cluster distant from the initial material, whereas the samples of SP1-4 ports from columns E and F clustered together, separated from the initial materials and samples from column G. Additionally, both richness and Shannon-Wiener diversity index (*H*') (Table S7) were 528 operational taxonomic units (OTUs) and *H*' = 3.6 in column G. However, compared with column G, columns E and F with Cu produced a decrease in both the OTU richness (526 and 431 OTUs, respectively) and the Shannon-Wiener diversity index (*H*' = 3.1 and 2.7, respectively). These data suggested that the presence of Cu reduced the diversity of the bacterial communities in columns E and F. Fig. 5c summarizes the differences in the total numbers of eubacterial 16S rDNA genes between the initial PRB materials and solid samples collected from sampling ports SP1-

SP4 of columns E, F and G. The levels of 16S rDNA genes in the latter samples were higher than in the initial materials in all cases, although the quantity was lower in column F than in columns E and G. These results can likely be attributed to the inhibition of microbial growth by the high iron concentration in column F (You et al., 2017). Additionally, the relatively high level of Cu ion in column F may also inhibit microbial growth. Vilchez et al. (2007) reported that the presence of Cu ion in the water had a negative effect on the biological activities of the biofilm. When Cu ion dissolves into water, it will behave toxicity to the living organism by damaging cell membrane, altering proteins and inhibiting their biological activity, interacting with nucleic acid and so forth (Li et al., 2021). Fujii and Fukunaga (2008) also reported that copper is known to show toxicity to brewer's yeast in a 3.2 mg/L of Cu ion solution and soil microbes at 6.4−64 mg/kg soil. The other study showed that the concentration of Cu ion decreasing the activated sludge activity to 50% (IC_{50}) recorded 3 mg/L (El Bestawy et al., 2013). Moreover, Wu et al. (2009) reported that the growth of microbes decreased when the pH was higher than 9.0. The possible local high pH generating by the Fe^0/H_2O system, attapulgite and Portland cement in column F may inhibit the microbial growth and biological enzyme activities (Zhang et al., 2018). An analysis of the relative abundance of bacterial taxa across columns E, F and G could provide a deep understanding of the microbes responsible for the proper functioning of the PRB. The biological degradation of *o*-NCB has been studied with different genera, such as *Clostridium* (Tartakovsky et al., 2001; Zhu et al., 2015) and *Pseudomonas* (Liu et al., 2005). As shown in Figs. 5d-f, columns E and F contained various bacteria capable of degrading *o*-NCB, such as *Clostridium* and *Pseudomonas*, but column G only included *Clostridium*. This variation could have been the result of the different reductants in materials E, F and G. Compared with the initial materials, the relative abundance of *o*-NCB-degrading bacteria in all three columns increased significantly, indicating that these genera were positively correlated with the efficient removal of *o*-NCB. Considering both the 16S rDNA genes and the relative abundance of various bacterial taxa, the bacteria capable of pollutant degradation were most plentiful in column E. The production of chloride ions was principally attributed to the action of these bacteria in column G, because dechlorination by Fe^0 did not occur (Figure S3). Therefore, biodegradation played an important role in the complete removal of *o*-NCB in these PRB systems. Figs. 6a-c demonstrate that the biomass levels predicted by the model were in reasonably good agreement with the experimental data. The majority of this biomass was supported by the presence of organic carbon (Figs. 6d-f) in columns E, F and G.

4. Conclusions

A novel PRB was evaluated with regard to the *in situ* remediation of groundwater contaminated with *o*-NCB. The resulting combination of iron-based reduction with microbial degradation was found to efficiently remove *o*-NCB. The rate of iron release from columns E and F was also shown to be faster than that from column G, although the extent of iron release had no significant effect on the removal of *o*-NCB by the PRB system. Organic carbon likely helped to maintain the population of microbes in these units in the presence of low *o*-NCB concentrations, and modelling results showed that organic carbon supported the majority of biomass in each column. The bacteria degrading *o*-NCB in columns E and F were determined to be different from those in column G, and the relative abundance of these bacteria in each column was higher than in the initial materials. The total concentration of bacteria responsible for remediation was highest in column E. Biodegradation played an important role in the complete removal of *o*-NCB from groundwater in the PRB systems. Assuming that carbon is released over a span of 20 years, the present modelling results generally fit well with the experimental data and support field-scale pilot testing of these materials for groundwater remediation.

Acknowledgements

We gratefully acknowledge the National Key R&D Program of China (2018YFD0800201 and 2018YFC1800806), the Environmental Protection Department of Jiangsu Province of China (Grant No. 2017001-1), and Jiangsu Academy of Environmental Industry and Technology (Grant No. BE2019624) for their financial support.

References

Acharya, K., Werner, D., Dolfing, J., Meynet, P., Tabraiz, S., Baluja, M.Q., Petropoulos, E., Mrozik, W., Davenport, R.J., 2019. The experimental determination of reliable biodegradation rates for mono-aromatics towards evaluating QSBR models. Water Res.

160, 278-287.

Agrawal, A., Tratnyek, P.G., 1995. Reduction of nitro aromatic compounds by zero-valent iron metal. Environ. Sci. Technol. 30, 153-160.

Ahmed, A.M., Tardy, V., Bonnineau, C., Billard, P., Pesce, S., Lyautey, E., 2020. Changes in sediment microbial diversity following chronic copper-exposure induce community copper-tolerance without increasing sensitivity to arsenic. J. Hazard. Mater. 391, 12.

Akobi, C., Hafez, H., Nakhla, G., 2017. Impact of furfural on biological hydrogen production kinetics from synthetic lignocellulosic hydrolysate using mesophilic and thermophilic mixed cultures. Int. J. Hydrog. Energy 42, 12159-12172.

Böhm, F., Sharma, V., Schwaab, G., Havenith, M., 2015. The low frequency modes of solvated ions and ion pairs in aqueous electrolyte solutions: iron (II) and iron (III) chloride. Phys. Chem. Chem. Phys. 17, 19582-19591.

Cao, J., Xu, R.F., Tang, H., Tang, S.S., Cao, M.H., 2011. Synthesis of monodispersed CMC-stabilized Fe-Cu bimetal nanoparticles for in situ reductive dechlorination of 1, 2, 4-trichlorobenzene. Sci. Total Environ. 409, 2336-2341.

Carboneras, B., Villasenor, J., Fernandez-Morales, F.J., 2017. Modelling aerobic biodegradation of atrazine and 2,4-dichlorophenoxy acetic acid by mixed-cultures. Bioresour. Technol. 243, 1044-1050.

Chang, N.B., Wen, D., McKenna, A.M., Wanielista, M.P., 2018. The impact of carbon source as electron donor on composition and concentration of dissolved organic nitrogen in biosorption-activated media for stormwater and groundwater co-treatment.

Environ. Sci. Technol. 52, 9380-9390.

Chen, Z.L., Shen, J.M., Li, X.Y., Qi, F., Xu, B.B., 2006. Ozonation degradation of p-nitrochlorobenzene in aqueous solution: kinetics and mechanism. J. Chem. Ind. Eng. (China) 57, 2439-2444.

Chen, Z.M., Wang, H.Y., Liu, X.W., Zhao, X.L., Lu, D.J., Zhou, J.M., Li, C.Z., 2017. Changes in soil microbial community and organic carbon fractions under short-term straw return in a rice-wheat cropping system. Soil Till. Res. 165, 121-127.

Chen, Z.Q., McTernan, W.F., 1992. Multi-substrate, multi-option groundwater transport model. J. Contam. Hydrol. 11, 215-244.

Cogle, A.L., Saffigna, P.G., Strong, W.M., 1989. Carbon transformations during wheat straw decomposition. Soil Biol. Biochem. 21, 367-372.

Dalaei, P., Bahreini, G., Nakhla, G., Santoro, D., Batstone, D., Hulsen, T., 2020. Municipal wastewater treatment by purple phototropic bacteria at low infrared irradiances using a photo-anaerobic membrane bioreactor. Water Res. 173, 12.

Dong, T.T., Luo, H.J., Wang, Y.P., Hu, B.J., Chen, H., 2011. Stabilization of Fe-Pd bimetallic nanoparticles with sodium carboxymethyl cellulose for catalytic reduction of para-nitrochlorobenzene in water. Desalination 271, 11-19.

Ebert, M., Kober, R., Parbs, A., Plagentz, V., Schafer, D., Dahmke, A., 2006. Assessing degradation rates of chlorinated ethylenes in column experiments with commercial iron materials used in permeable reactive barriers. Environ. Sci. Technol. 40, 2004-2010.

El Bestawy, E., Helmy, S., Hussein, H., Fahmy, M., 2013. Optimization and/or acclimatization of activated sludge process under heavy metals stress. World J.

Microbiol. Biotechnol. 29, 693-705.

Esfahani, A.R., Firouzi, A.F., Sayyad, G., Kiasat, A.R., 2014. Transport and retention of polymer-stabilized zero-valent iron nanoparticles in saturated porous media: effects of initial particle concentration and ionic strength. J. Ind. Eng. Chem. 20, 2671-2679.

Fagnano, M., Agrelli, D., Pascale, A., Adamo, P., Fiorentino, N., Rocco, C., Pepe, O., Ventorino, V., 2020. Copper accumulation in agricultural soils: risks for the food chain and soil microbial populations. Sci. Total Environ. 734, 11.

Fang, L.P., Xu, C.H., Zhang, W.B., Huang, L.Z., 2018. The important role of polyvinylpyrrolidone and Cu on enhancing dechlorination of 2,4-dichlorophenol by Cu/Fe nanoparticles: performance and mechanism study. Appl. Surf. Sci. 435, 55-64.

Farrell, J., Kason, M., Melitas, N., Li, T., 2000. Investigation of the long-term performance of zero-valent iron for reductive dechlorination of trichloroethylene. Environ. Sci. Technol. 34, 514-521.

Fujii, K., Fukunaga, S., 2008. Isolation of highly copper-tolerant fungi from the smelter of the Naganobori copper mine, an historic mine in Japan. J. Appl. Microbiol. 105, 1851-1857.

Gao, J., Li, J., Zuo, X.Y., Yuan, H.R., Liu, Y.P., Li, X.J., 2020. Effect of biochar-addition on anaerobic digestion performance of wheat straw and its microbial community structure. China Biogas 38, 14-20.

Gibert, O., Assal, A., Devlin, H., Elliot, T., Kalin, R.M., 2019. Performance of a field-scale biological permeable reactive barrier for in-situ remediation of nitrate-contaminated groundwater. Sci. Total Environ. 659, 211-220.

Henderson, A.D., Demond, A.H., 2007. Long-term performance of zero-valent iron permeable reactive barriers: a critical review. Environ. Eng. Sci. 24, 401-423.

Hosseini, S.M., Ataie-Ashtiani, B., Kholghi, M., 2011. Nitrate reduction by nano-Fe/Cu particles in packed column. Desalination 276, 214-221.

Huang, B.B., Qian, W.T., Yu, C.X., Wang, T., Zeng, G.M., Lei, C., 2016. Effective catalytic hydrodechlorination of o-, p- and m-chloronitrobenzene over Ni/Fe nanoparticles: effects of experimental parameter and molecule structure on the reduction kinetics and mechanisms. Chem. Eng. J. 306, 607-618.

Karami, S., Zeynizadeh, B., Shokri, Z., 2018. Cellulose supported bimetallic Fe-Cu nanoparticles: a magnetically recoverable nanocatalyst for quick reduction of nitroarenes to amines in water. Cellulose 25, 3295-3305.

King, S., Courvoisier, P., Guiot, S., Barrington, S., 2012. In-storage psychrophilic anaerobic digestion: acclimated microbial kinetics. Environ. Technol. 33, 1763-1772.

Kitcher, E., Braida, W., Koutsospyros, A., Pavlov, J., Su, T.L., 2017. Characteristics and products of the reductive degradation of 3-nitro-1,2,4-triazol-5-one (NTO) and 2,4-dinitroanisole (DNAN) in a Fe-Cu bimetal system. Environ. Sci. Pollut. Res. 24, 2744-2753.

Kong, W.Q., Lin, J.Y., He, X., Cheng, Y.Y., Zhang, X.S., Deng, G.Z., Han, R.S., Wu, C., 2017. Reduction pathway and mechanism of chloronitrobenzenes synergistically catalyzed by bioPd and Shewanella oneidensis MR-1 assisted by calculation. Chemosphere 187, 62-69.

Kuhlmann, A., Hegemann, W., 1997. Degradation of monochloronitrobenzenes by

Pseudomonas acidovorans CA50. Acta Hydroch. Hydrob. 25, 298-305.

la Cecilia, D., Maggi, F., 2016. Kinetics of atrazine, deisopropylatrazine, and deethylatrazine soil biodecomposers. J. Environ. Manage. 183, 673-686.

Lashermes, G., Bleuze, L., Recous, S., Voinot, R., Lafolie, F., Chabbert, B., 2020. Multiscale modeling of microbial degradation of outer tissues of fiber-crop stems during the dew retting process. Bioresour. Technol. 311, 10.

Li, B.Z., Ouyang, Y.B., Haider, Z., Zhu, Y.H., Qiu, R., Hu, S.G., Niu, H.L., Zhang, Y., Chen, M., 2021. One-step electrochemical deposition leading to superhydrophobic matrix for inhibiting abiotic and microbiologically influenced corrosion of Cu in seawater environment. Colloid Surf. A-Physicochem. Eng. Asp. 616, 13.

Li, B.Z., Xu, X.Y., Zhu, L., 2009. Ozonation of chloronitrobenzenes in aqueous solution: kinetics and mechanism. J. Chem. Technol. Biotechnol. 84, 167-175.

Li, X.Y., Liu, Y.B., Zhang, W.M., Zhang, M., Li, X., Yang, B., Hua, R., 2017. Effects of ionic strength,temperature and pH on enrichment of Th(IV) in aqueous solution by nanoscale zero-valent iron. At. Energy Sci. Technol. 51, 975-980.

Lin, H.Z., Zhu, L.A., Xu, X.Y., Zang, L.L., Kong, Y., 2011. Reductive transformation and dechlorination of chloronitrobenzenes in UASB reactor enhanced with zero-valent iron addition. J. Chem. Technol. Biotechnol. 86, 290-298.

Liu, C.C., Chen, X.H., Mack, E.E., Wang, S., Du, W.C., Yin, Y., Banwart, S.A., Guo, H.Y., 2019. Evaluating a novel permeable reactive bio-barrier to remediate PAH-contaminated groundwater. J. Hazard. Mater. 368, 444-451.

Liu, H., Wang, S.J., Zhou, N.Y., 2005. A new isolate of Pseudomonas stutzerithat degrades 2-chloronitrobenzene. Biotechnol. Lett. 27, 275-278.

Liu, Z.H., Guo, W.L., Han, X.M., Li, X.H., Zhang, K., Qiao, Z.M., 2016. In situ remediation of ortho-nitrochlorobenzene in soil by dual oxidants (hydrogen peroxide/persulfate). Environ. Sci. Pollut. Res. 23, 19707-19712.

Malaguerra, F., Chambon, J.C., Bjerg, P.L., Scheutz, C., Binning, P.J., 2011. Development and sensitivity analysis of a fully kinetic model of sequential reductive dechlorination in groundwater. Environ. Sci. Technol. 45, 8395-8402.

Moustafa, M., 2019. Drift pump back test for residence time distribution in engineered treatment system. Bioremediat. J. 1-10.

Nguyen, V.K., Park, Y., Yu, J., Lee, T., 2016. Microbial selenite reduction with organic carbon and electrode as sole electron donor by a bacterium isolated from domestic wastewater. Bioresour. Technol. 212, 182-189.

Ouyang, F., Ji, M., Zhai, H.Y., Dong, Z., Ye, L., 2016. Dynamics of the diversity and structure of the overall and nitrifying microbial community in activated sludge along gradient copper exposures. Appl. Microbiol. Biotechnol. 100, 6881-6892.

Pan, Y., Sun, L.P., Chen, X.Y., Lin, M.Y., 2019. Removal of 2,4-dichlorophenol from groundwater by PRB simulated by CMC modified nanoscale Fe/Cu bimetal. China Environ. Sci. 39, 3789-3796.

Park, H.S., Lim, S.J., Chang, Y.K., Livingston, A.G., Kim, H.S., 1999. Degradation of chloronitrobenzenes by a coculture of Pseudomonas putida and a Rhodococcussp. Appl. Environ. Microbiol. 65, 1083-1091.

Qiu, H., Ni, W.X., Zhang, H.H., Chen, K., Yu, J.C., 2020. Fabrication and evaluation of a regenerable HFO-doped agricultural waste for enhanced adsorption affinity towards phosphate. Sci. Total Environ. 703, 135493.

Ren, Y., Yang, J.H., Li, J., Lai, B., 2017. Strengthening the reactivity of Fe^0/(Fe/Cu) by premagnetization: implications for nitrate reduction rate and selectivity. Chem. Eng. J. 330, 813-822.

Schafer, D., Schafer, W., Kinzelbach, W., 1998. Simulation of reactive processes related to biodegradation in aquifers-1. Structure of the three-dimensional reactive transport model. J. Contam. Hydrol. 31, 167-186.

Shih, Y.H., Chen, Y.C., Chen, M.Y., Tai, Y.T., Tso, C.P., 2009. Dechlorination of hexachlorobenzene by using nanoscale Fe and nanoscale Pd/Fe bimetallic particles. Colloid Surf. A-Physicochem. Eng. Asp. 332, 84-89.

Tartakovsky, B., Manuel, M.F., Beaumier, D., Greer, C.W., Guiot, S.R., 2001. Enhanced selection of an anaerobic pentachlorophenol-degrading consortium. Biotechnol. Bioeng. 73, 476-483.

Vasiliadou, I.A., Chowdhury, A., Akratos, C.S., Tekerlekopoulou, A.G., Pavlou, S., Vayenas, D.V., 2015. Mathematical modeling of olive mill waste composting process. Waste Manage. 43, 61-71.

Verce, M.F., Ulrich, R.L., Freedman, D.L., 2000. Characterization of an isolate that uses vinyl chloride as a growth substrate under aerobic conditions. Appl. Environ. Microbiol. 66, 3535-3542.

Vilchez, R., Pozo, C., Gomez, M.A., Rodelas, B., Gonzalez-Lopez, J., 2007. Dominance of sphingomonads in a copper-exposed biofilm community for groundwater treatment. Microbiol.-(UK) 153, 325-337.

Wu, H.Z., Wei, C.H., Wang, Y.Q., He, Q.C., Liang, S.Z., 2009. Degradation of o-chloronitrobenzene as the sole carbon and nitrogen sources by Pseudomonas putida OCNB-1. J. Environ. Sci. 21, 89-95.

Xu, H.B., Zhao, D.Y., Li, Y.J., Liu, P.Y., Dong, C.X., 2014. Enhanced degradation of ortho-nitrochlorobenzene by the combined system of zero-valent iron reduction and persulfate oxidation in soils. Environ. Sci. Pollut. Res. 21, 5132-5140.

Xu, S.P., Jaffe, P.R., Mauzerall, D.L., 2007. A process-based model for methane emission from flooded rice paddy systems. Ecol. Model. 205, 475-491.

Xu, X.Y., Lin, H.Z., Zhu, L., Yang, Y.N., Feng, J.Q., 2011. Enhanced biodegradation of 2-chloronitro-benzene using a coupled zero-valent iron column and sequencing batch reactor system. J. Chem. Technol. Biotechnol. 86, 993-1000.

Xu, Z.H., Sun, Z.H., Zhou, Y.W., Zhang, D.F., Gao, Y.Q., Huang, Y.X., Chen, W.F., 2020. Enhanced hydrodechlorination of p-chloronitrobenzene by a GAC-Fe-Cu ternary micro-electrolysis system: synergistic effects and removal mechanism. Sep. Purif. Technol. 237, 13.

Yin, W.Z., Wu, J.H., Li, P., Lin, G.H., Wang, X.D., Zhu, B., Yang, B., 2012. Reductive transformation of pentachloronitrobenzene by zero-valent iron and mixed anaerobic culture. Chem. Eng. J. 210, 309-315.

You, G.X., Wang, P.F., Hou, J., Wang, C., Xu, Y., Miao, L.Z., Lv, B.W., Yang, Y.Y., Zhang, F., 2017. The use of zero-valent iron (ZVI)-microbe technology for wastewater treatment with special attention to the factors influencing performance: a critical review.

Crit. Rev. Environ. Sci. Technol. 47, 877-907.

Zhang, D.J., Shen, J.Y., Shi, H.F., Su, G.Y., Jiang, X.B., Li, J.S., Liu, X.D., Mu, Y., Wang, L.J., 2019a. Substantially enhanced anaerobic reduction of nitrobenzene by biochar stabilized sulfide-modified nanoscale zero-valent iron: process and mechanisms. Environ. Int. 131, 10.

Zhang, D.L., Zeng, X.Y., Yu, Z.Q., Sheng, G.Y., Fu, J.M., 2011. Determination of nitrobenzenes and nitrochlorobenzenes in water samples using dispersive liquid-liquid microextraction and gas chromatography-mass spectrometry. Anal. Methods 3, 2254-2260.

Zhang, W.C., Zhu, J.Q., Zhou, X.G., Li, F.H., 2018. Effects of shallow groundwater table and fertilization level on soil physico-chemical properties, enzyme activities, and winter wheat yield. Agric. Water Manage. 208, 307-317.

Zhang, W.Y., Qian, L.B., Ouyang, D., Chen, Y., Han, L., Chen, M.F., 2019b. Effective removal of Cr(VI) by attapulgite-supported nanoscale zero-valent iron from aqueous solution: enhanced adsorption and crystallization. Chemosphere 221, 683-692.

Zhu, L., Jin, J., Lin, H.Z., Gao, K.T., Xu, X.Y., 2015. Succession of microbial community and enhanced mechanism of a ZVI-based anaerobic granular sludge process treating chloronitrobenzenes wastewater. J. hazard. mater. 285, 157-166.

Zhu, L., Lin, H.Z., Qi, J.Q., Xu, X.Y., 2013. Enhanced transformation and dechlorination of p-chloronitrobenzene in the combined ZVI-anaerobic sludge system. Environ. Sci. Pollut. Res. 20, 6119-6127.

Ziganshin, A.M., Liebetrau, J., Pröter, J., Kleinsteuber, S., 2013. Microbial community structure and dynamics during anaerobic digestion of various agricultural waste materials. Appl. Microbiol. Biotechnol. 97, 5161-5174.

Table Captions

Table 1. Stoichiometric relationships for the geochemical reactions simulated in the model.

Reaction	Stoichiometry
Organic carbon consumption	$3CH_2O + H_2O \rightarrow CH_3COOH + CO_2 + 2H_2$
Iron corrosion	$Fe^0 + 2H_2O \rightarrow Fe^{2+} + H_2 + 2OH^-$
	$Fe^{2+} + 2OH^- \rightarrow Fe(OH)_2$
	$2Fe^{2+} + H_2O \rightarrow 2Fe^{3+} + 2H_2 + 2OH^-$
	$2Fe^{3+} + Fe^0 \rightarrow 3Fe^{2+}$
o-NCB transformation	*o*-NCB + $3H_2 \rightarrow$ *o*-CAN + $2H_2O$
	2*o*-CAN + $H_2 \rightarrow$ 2AN + $2Cl^-$

Table 2. Modelling parameters used for the column experiments.

Parameter	Column E	Column F	Column G
Iron reduction	[a]$k_1 = 1.61\times10^{-5}$; [a]$k_2 = 2.76\times10^{-7}$	[a]$k_1 = 2.00\times10^{-5}$; [a]$k_2 = 3.42\times10^{-7}$	[a]$k_1 = 6.42\times10^{-6}$
Microbial degradation for *o*-NCB	[i]$\mu_{max} = 2.1\times10^{-4}$; [c]$K_{H_2} = 1.39\times10^{-7}$; [c]$K_s = 9.32\times10^{-6}$; [c]$K_1 = 1\times10^{-4}$; [b]$Y_X = 0.778$	[g]$\mu_{max} = 1.93\times10^{-4}$; [c]$K_{H_2} = 1.39\times10^{-7}$; [c]$K_s = 9.32\times10^{-6}$; [c]$K_1 = 1\times10^{-4}$; [b]$Y_X = 0.778$	[j]$\mu_{max} = 5.9\times10^{-4}$; [c]$K_{H_2} = 1.39\times10^{-7}$; [c]$K_s = 9.32\times10^{-6}$; [c]$K_1 = 1\times10^{-4}$; [b]$Y_X = 0.778$
Organic carbon consumption	[d]$\mu_{max} = 1.27\times10^{-7}$; [b]$K_{oc} = 8.03\times10^{-3}$; [e]$Y_X = 0.954$	[f]$\mu_{max} = 5.56\times10^{-8}$; [g]$K_{oc} = 2.609\times10^{-3}$; [e]$Y_X = 0.954$	[d]$\mu_{max} = 1.27\times10^{-7}$; [g]$K_{oc} = 6.477\times10^{-3}$; [e]$Y_X = 0.954$
Biomass	[h]$b = 1.16\times10^{-8}$	[h]$b = 1.16\times10^{-8}$	[h]$b = 1.16\times10^{-8}$

[a]Data obtained based on Table S4; [b]Data from (la Cecilia and Maggi, 2016); [c]Data from (Malaguerra et al., 2011); [d]Data from (Carboneras et al., 2017); [e]Data from (Vasiliadou et al., 2015); [f]Data from (Verce et al., 2000); [g]Data from (Akobi et al., 2017); [h]Data from (Chen and McTernan, 1992); [i]Data from (Acharya et al., 2019); [j]Data from (Schafer et al., 1998).

Figure Captions

Fig. 1. A conceptual model including iron reduction, microbial degradation and the consumption of dissolved organic carbon during the experimental process.

Fig. 2. Simulated (lines) and experimental (symbols) results for variations in (a) *ortho*-nitrochlorobenzene, (b) *o*-chloroaniline, (c) chloride ion, (d) total iron, and (e) total organic carbon as functions of time in the effluents of columns E, F and G.

Fig. 3. ESEM images of materials E, F and G before (E0, F0 and G0) and after (E1, F1 and G1) the 460 d column experiments. EDS mapping images showing the distributions of (a-f) C, (g-l) Fe and (m-p) Cu.

Fig. 4. XPS high-resolution spectra of Fe 2p in PRB materials E, F and G before and after column experiments.

Fig. 5. (a) Composition of the bacterial community at phylum level in the initial PRB materials and in solid samples from columns E, F and G. (b) Principal coordinates analysis of bacterial community structures using unweighted UniFrac distances. (c) Total quantities of eubacterial 16S rDNA genes. Relative abundance values for bacteria having a degradation effect at the genus level in the initial PRB materials and in solid samples collected from ports SP1-4 of columns (d) E, (e) F, and (f) G.

Fig. 6. Comparison of simulated and experimental results for biomass from the initial materials and samples acquired from ports SP1-4 in columns (a) E, (b) F, and (c) G. The simulated biomass supported by *o*-NCB and organic carbon (OC) in columns (d) E, (e) F, and (f) G.

Fig. 1

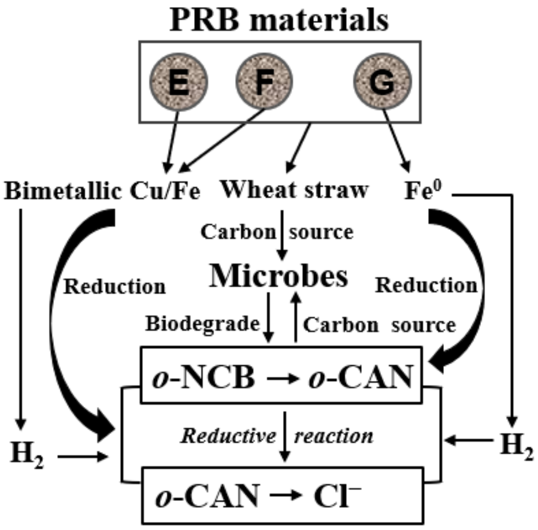
PRB materials
E
F
G
Bimetallic Cu/Fe
Wheat straw
Fe^0
Carbon source
Microbes
Reduction
Reduction
Biodegrade
Carbon source
o-NCB → o-CAN
Reductive reaction
H_2
H_2
o-CAN → Cl$^-$

Fig. 2

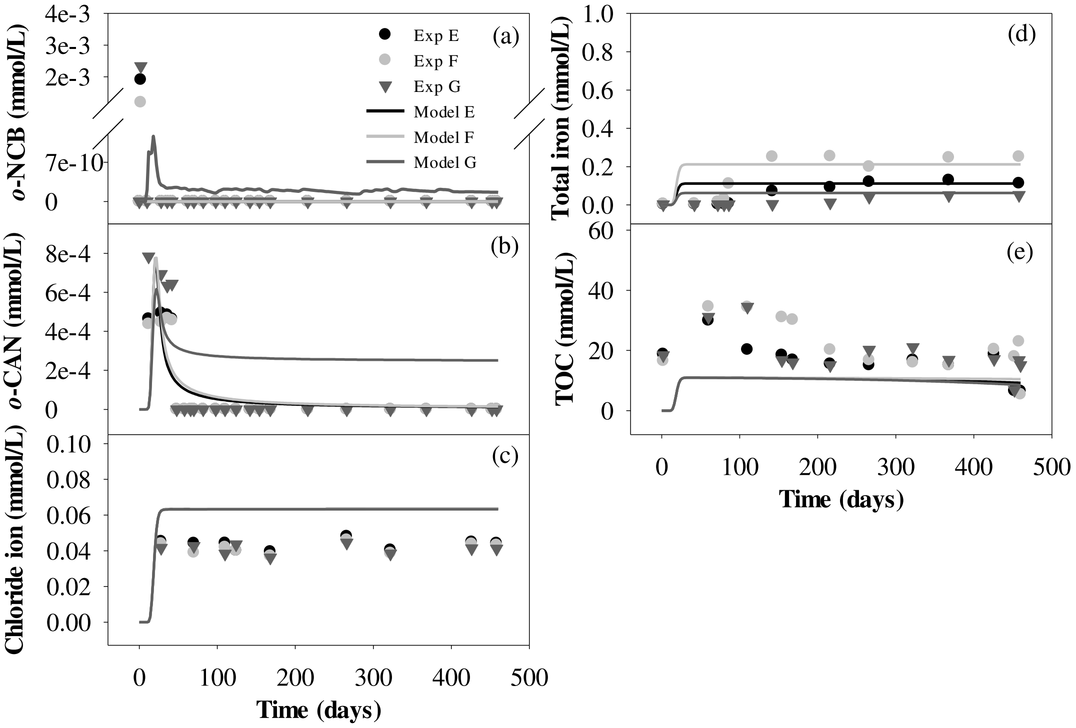
(a)
(b)
(c)
(d)
(e)
Exp E
Exp F
Exp G
Model E
Model F
Model G
o-NCB (mmol/L)
4e-3
3e-3
2e-3
7e-10
0
o-CAN (mmol/L)
8e-4
6e-4
4e-4
2e-4
0
Chloride ion (mmol/L)
0.10
0.08
0.06
0.04
0.02
0.00
Total iron (mmol/L)
1.0
0.8
0.6
0.4
0.2
0.0
TOC (mmol/L)
60
40
20
0
0
100
200
300
400
500
Time (days)

Fig. 3

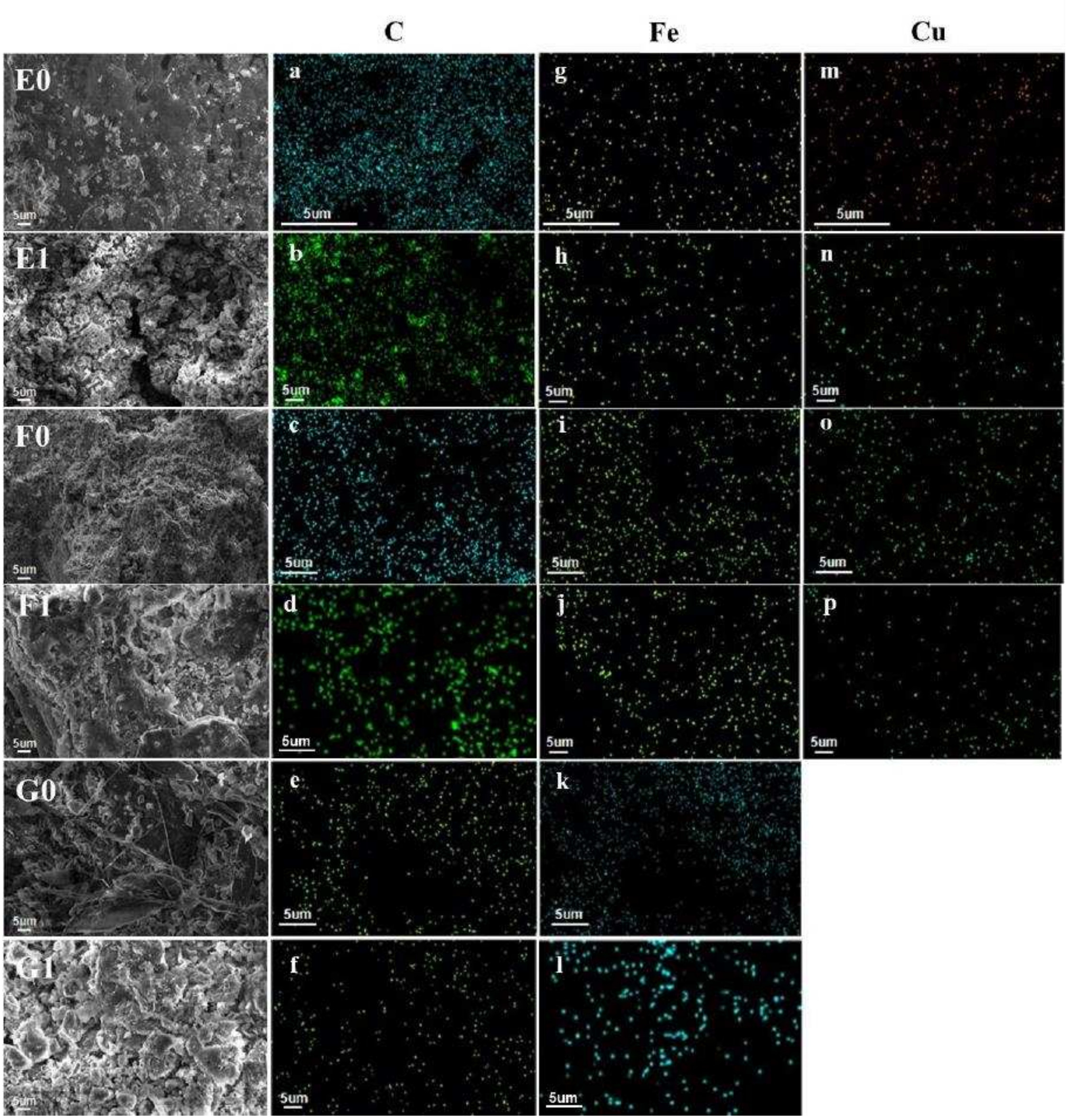

Fig. 4

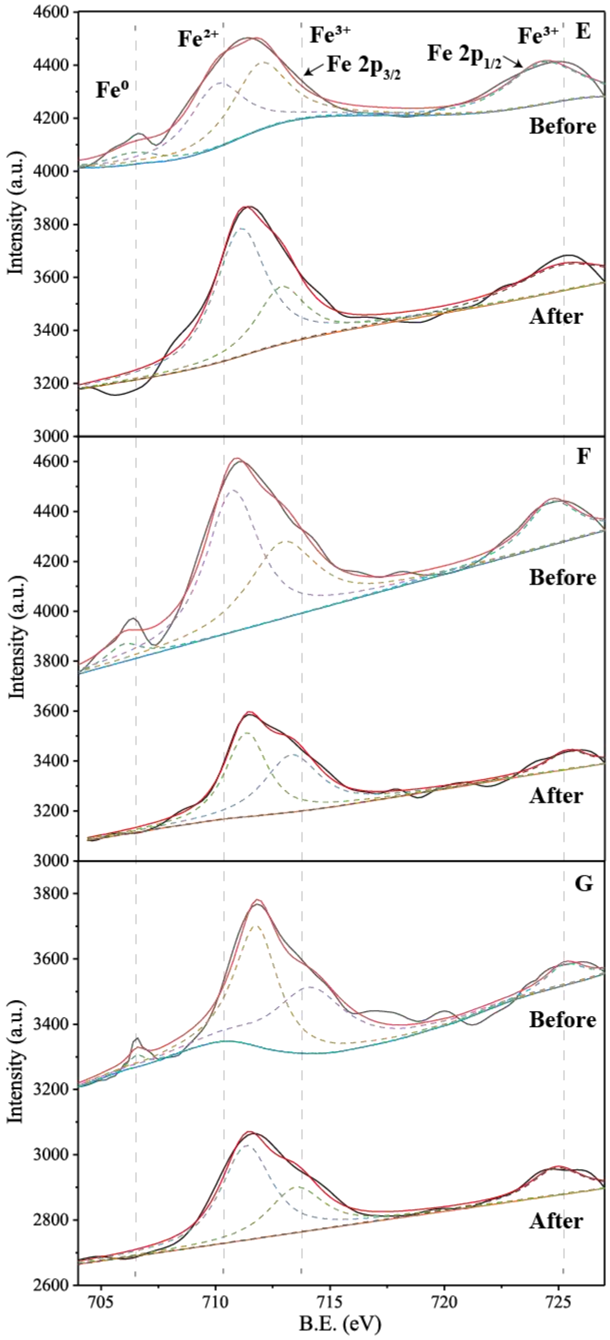
Fe0
Fe2+
Fe3+
Fe 2p3/2
Fe 2p1/2
Fe3+
E
Before
After
F
Before
After
G
Before
After
Intensity (a.u.)
Intensity (a.u.)
Intensity (a.u.)
4600
4400
4200
4000
3800
3600
3400
3200
3000
4600
4400
4200
4000
3800
3600
3400
3200
3000
3800
3600
3400
3200
3000
2800
2600
705
710
715
720
725
B.E. (eV)

Fig. 5

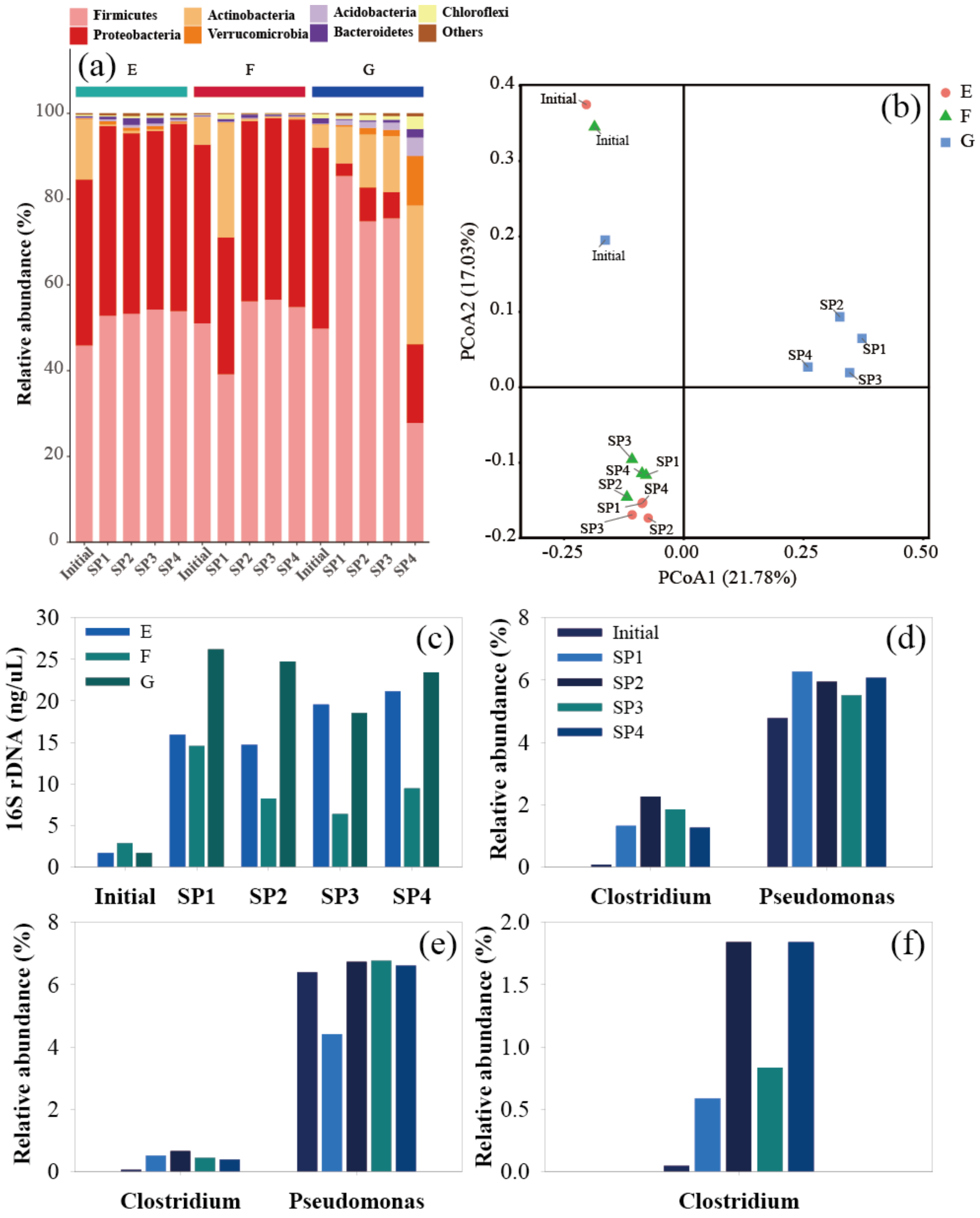
Firmicutes
Proteobacteria
Actinobacteria
Verrucomicrobia
Acidobacteria
Bacteroidetes
Chloroflexi
Others
(a)
E
F
G
Relative abundance (%)
0
20
40
60
80
100
Initial
SP1
SP2
SP3
SP4
(b)
PCoA2 (17.03%)
PCoA1 (21.78%)
0.4
0.3
0.2
0.1
0.0
-0.1
-0.2
-0.25
0.00
0.25
0.50
(c)
16S rDNA (ng/uL)
0
5
10
15
20
25
30
(d)
Clostridium
Pseudomonas
0
2
4
6
8
(e)
(f)
0.0
0.5
1.0
1.5
2.0

749 **Fig. 6**

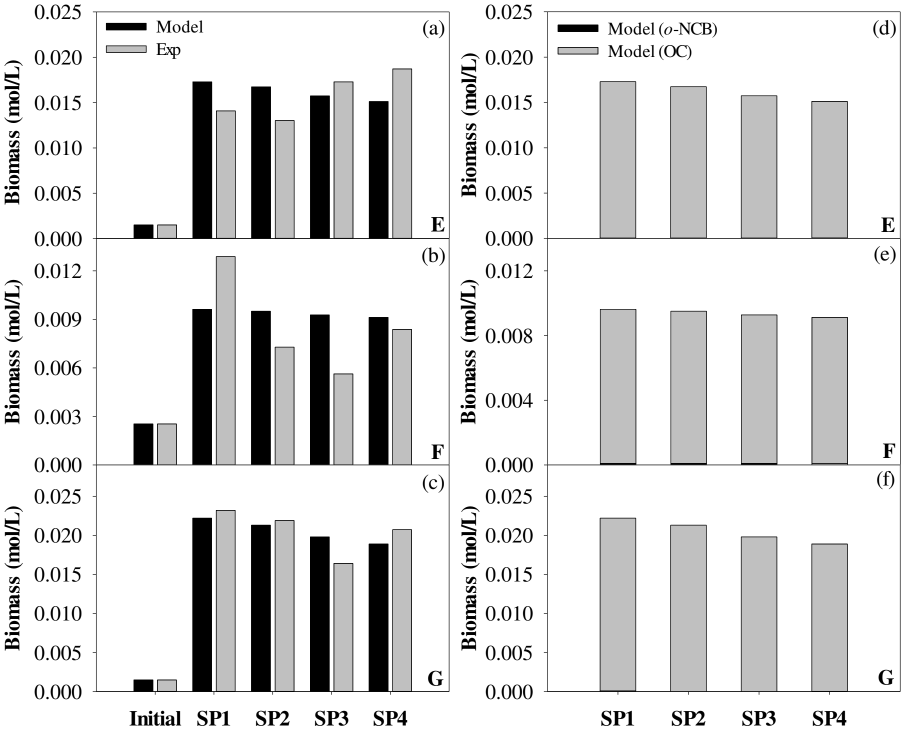

Model
Exp
Model (o-NCB)
Model (OC)
(a)
(b)
(c)
(d)
(e)
(f)
E
F
G
Biomass (mol/L)
0.025
0.020
0.015
0.010
0.005
0.000
0.012
0.009
0.006
0.003
0.008
0.004
Initial
SP1
SP2
SP3
SP4

750